Free-Lagrange Simulations of Shock/Bubble Interaction in Shock Wave Lithotripsy

Ahmad R. Jamaluddin[1], Graham J. Ball[2], and Timothy G. Leighton[3]

[1] School of Engineering Sciences, University of Southampton, Highfield, SO17 1BJ, UK
[2] Atomic Weapons Establishment, Aldermaston, Reading, RG7 4PR, UK
[3] Institute of Sound and Vibration Research, University of Southampton, Highfield, SO17 1BJ, UK

Abstract. A Free-Lagrange CFD code is used to model the near-field interactions between a lithotripter shock wave and a single spherical air bubble in water in axisymmetric form. The shock wave interaction causes the bubble to collapse and undergo jetting which consequently generates a blast wave into the surrounding water due to a liquid-liquid impact. Following impact, the bubble attains a toroidal shape and undergoes subsequent expansion and collapse. A detailed description of the shock/bubble interaction event is given, which includes both primary and secondary collapse. Near-field pressure-time histories are presented.

1 Introduction

Studies of SWL have shown that cavitation bubbles are induced *in vivo* near the lithotripter focus by the tensile stress of lithotripter shock wave pulses [1]. An idealised lithotripter shock profile consists of a leading shock front with peak positive pressure, P^+, up to $100\,MPa$, followed by a tensile wave with a peak negative pressure, P^-, down to $-10\,MPa$, and a total pulse duration of 3 to $7\,\mu$s [2]. The collapse of such cavitation bubbles near a solid surface [3] or by an incident shock [4] can produce a liquid jet. The mechanical stresses generated by the shock-bubble interaction and subsequent jet impact on the kidney stone have been identified as a possible mechanism of kidney stone fragmentation during lithotripsy [5]. However, the violent collapse of cavitation bubbles also causes collateral damage to the kidneys as well as the surrounding tissue [6]. The costs and benefits of the treatment are therefore highly dependent on whether the focal point of the lithotripter generator is accurately targeted on the stone.

Despite these findings, current commercial lithotripters are not equipped with any means to assess qualitatively the cavitation activity in patients during clinical lithotripsy. One means of detecting the presence of cavitation bubbles is to measure their acoustic emissions [7,8]. In an attempt to explore the feasibility of assessing inertial cavitation *in vivo* during SWL based on acoustic measurements, Zhong *et al.* [9] studied the dynamics of cavitation *in vitro* using high-speed photography and measured the associated acoustic emission in water emanating from the focus of an electrohydraulic shock wave lithotripter. A clear correlation between the dynamics of lithotripsy-induced cavitation bubbles and

resultant acoustic emission was identified. On the other hand, Cunningham *et al.* [8] used time-frequency analysis to quantify cavitation activity *in vivo* and used the time of the detected acoustic emissions to infer a value for the radius of stable bubble. However, in most experimental work, understanding of the fluid mechanics involved is incomplete owing to the limited temporal and spatial resolution of available experimental diagnostics.

The main objective of the present work is to simulate the cavitation events of shock-induced bubble collapse by lithotripter shock wave using the Free-Lagrange method in axisymmetric form and to predict the acoustic emission in the near field.

2 Numerical method

The numerical simulation is performed using the Free-Lagrange (FL) code, *Vucalm*, developed by Ball [10]. The code solves the unsteady, inviscid and compressible Euler equations, in axisymmetric form. The flow solver is of Godunov-type, and nominal 2^{nd} order spatial accuracy is achieved using a piece-wise linear reconstruction of conserved variables. In order to ensure monotonicity at steep gradients, a MUSCL slope limiter is used.

The FL method uses a fully unstructured Lagrangian mesh in which the connectivity is allowed to change freely as the flow evolves, and is thereby suitable for highly deforming flows. The mesh is constructed using a Voronoi diagram. The working fluid is divided into discrete cells, each containing a single particle which carries information of fluid type, properties, coordinates and flow conditions. The mass and fluid type of each mesh cell is assigned from the start of the simulation and never changes. There are no mixed cells and hence the material interfaces are always sharply resolved. The code employs a simple interface smoothing algorithm which acts as a form of artificial surface tension [11]. This prevents numerically seeded Richtmyer-Meshkov instability occurring on the the interface when strongly shocked. The water is represented by the Tait equation of state, while the ideal gas equation is used for air. The code uses the HLLC approximate Riemann solver at gas/gas interfaces and an exact solver at gas/water and water/water cell interfaces [12].

3 Problem specification

The problem studied in the present work comprises a single spherical air bubble immersed in water (Fig. 1). The initial density for air and water are $1.2246\,kgm^{-3}$ and $1000\,kgm^{-3}$ respectively while the initial temperature and pressure for both fluids are $0.1\,MPa$ and $288.15\,K$. The initial air bubble radius $R_0 = 0.06\,mm$ [7], which was chosen to be typical of a secondary stable bubble[1]. A

[1] A secondary stable bubble is a bubble which has been formed as a result of the interaction of a preceding lithotripter pulse with a cavitation nucleus, and which has reached a state of mechanical equilibrium with the surrounding fluid.

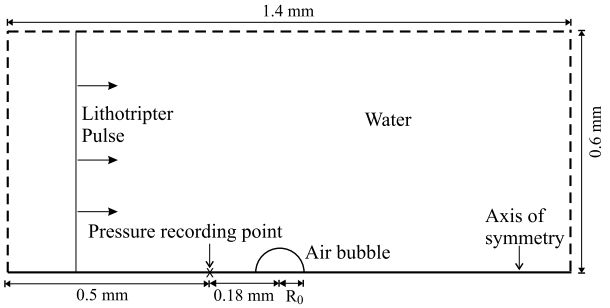

Fig. 1. The geometry of the problem

planar lithotripter pulse, with $P^+ = 90\,MPa$ and $P^- = -10\,MPa$, propagates through the water from left to right. Only half of the problem is simulated. The lower domain boundary represents the axis of symmetry. All elapsed times are measured from the first shock/bubble impact.

The lithotripter pulse is introduced by imposing a time-dependent pressure boundary condition on the left boundary. The top and right boundaries are non-reflecting at all times. A pressure recording point is positioned on the axis of rotation, $0.18\,mm$ from the initial bubble centre in order to register pressure pulses produced by cavitation event. A mesh of approximately $4{\times}10^4$ cells has been used.

4 Results and discussion

As a result of the profound acoustic impedance mismatch, a relatively weak shock is transmitted into the air bubble when the lithotripter shock (IS) hits the left bubble wall, whilst a strong expansion fan is produced in the water, running leftwards and upwards (EX in Fig. 3(a)). The high particle velocity behind the incident shock causes the bubble wall to deform to the right. At $t = 0.07\,\mu$s, the incident shock has traversed almost the full bubble width (Fig. 2(a)). The interaction between the shock and expansion waves originating at the bubble surface results in weakening and curvature of the shock. The air shock propagates more slowly and decouples from the incident shock. The deformation of the upstream bubble wall continues after the incident shock has passed because of the inertia of the water.

Interaction of the lithotripter pulse with the bubble causes it to collapse rapidly. The pressure gradient in the water near the upstream bubble increases as time progresses. It is clear from Fig. 2 that the collapse is asymmetric as the downstream bubble wall remains stationary up to about $t = 0.11\,\mu$s (Fig. 2(b)). At about $t = 0.20\,\mu$s (Fig. 2(c)), the upstream bubble wall starts to involute to form a distinct jet of liquid running to the right along the symmetry axis. The motion of the bubble during this phase is controlled almost exclusively by the inertia of the water. The liquid jet continues to accelerate and hits the downstream

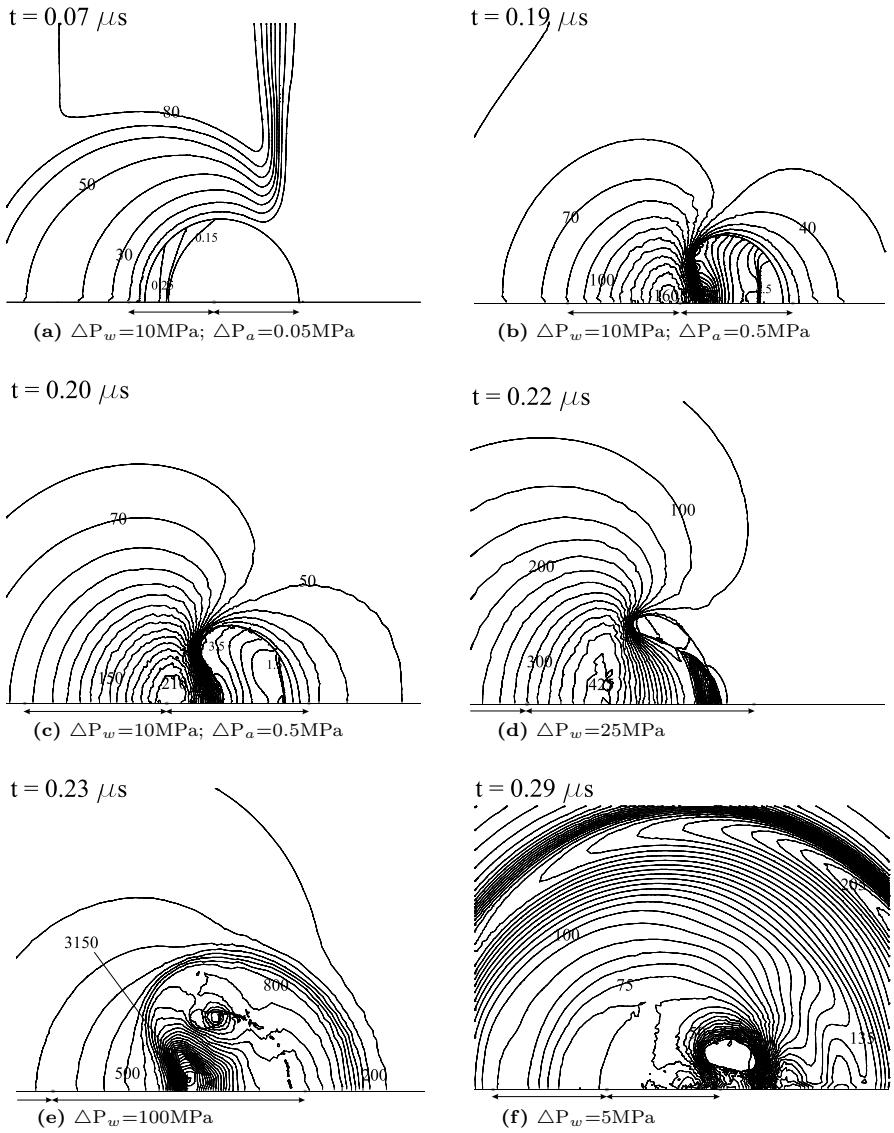

(a) $\triangle$P$_w$=10MPa; $\triangle$P$_a$=0.05MPa
(b) $\triangle$P$_w$=10MPa; $\triangle$P$_a$=0.5MPa
(c) $\triangle$P$_w$=10MPa; $\triangle$P$_a$=0.5MPa
(d) $\triangle$P$_w$=25MPa
(e) $\triangle$P$_w$=100MPa
(f) $\triangle$P$_w$=5MPa

Fig. 2. Pressure contours for an air bubble impacted by a lithotripter shock with $P^+ = 90\,MPa$ and $P^- = 10\,MPa$. Horizontal arrows indicate initial position and size of bubble. $\triangle$P$_w$ and $\triangle$P$_a$ indicate the increments between contours in the water and air respectively

wall at about $t = 0.22\,\mu$s, isolating a lobe of trapped and highly compressed gas which form a toroid in three dimensions (Fig. 2(d)). The variation of jet velocity with time is shown in Fig. 3(b). The jet continues to accelerate as it pierces the

bubble, reaching a maximum of over $1200\,ms^{-1}$ immediately prior to jet impact. It is believed that high-speed jets of this type play a primary role in cavitation erosion [13] as well as formation of circular pits and indentation on metal foils [1]. It is clear that the motion of the primary collapse is driven solely by the compressive component of the lithotripter pulse as the bubble does not encounter the tensile portion of the pulse before the primary collapse is complete.

The impact of the jet on the downstream bubble wall produces an intense blast wave in the surrounding water. It also leads to the creation of bubble fragments (Fig. 2(e)). These fragments may coalesce with the main cavity or act as nuclei for further cavitation events. The peak overpressure exceeds $1.0\,GPa$. As a result of the high velocity of the jet fluid, the blast wave advances relatively slowly to the left below the bubble. Consequently, the blast front is asymmetric. The interaction between the high-momentum liquid jet and the downstream low-momentum water produces a strong vortex flow.

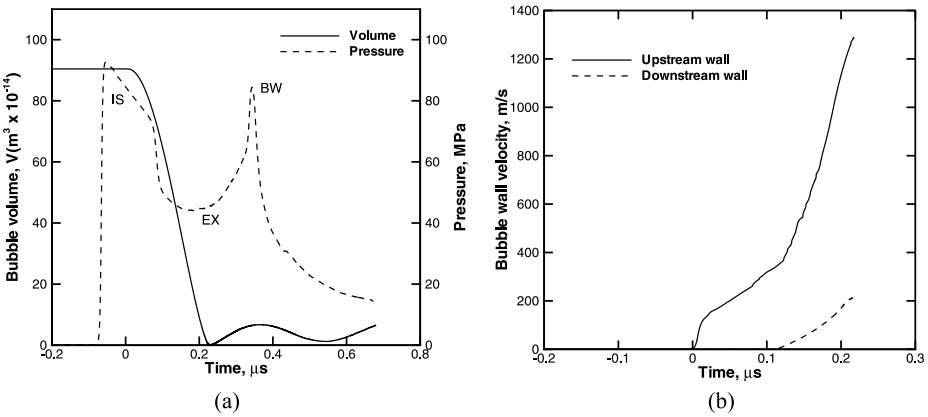

Fig. 3. (a) Pressure and bubble volume time history. Pressure is measured at point 'x' on Fig. 1. IS - Lithotripter shock, EX - Expansion waves, BW - Blast wave **(b)** Liquid jet velocity history

In Fig. 2(e), the air cavity is drawn into the vortex core while the blast wave continues to propagate outwards radially from the bubble. The blast wave produces a sharp peak (BW) on the pressure-time history curve recorded at the pressure point (Fig. 3(a)). The strength of the blast wave decreases as it propagates into the surrounding water. The radiated blast wave could explain the large pressure spikes recorded by Zhong *et al.* [9] near primary collapse in their experimental studies.

The time history of the cavity volume is shown in Fig. 3(a). The volume reduces linearly with time from shock-bubble impact, until the first minimum at $t \approx 0.22\,\mu$s. The end of the linear phase correlates with the liquid jet impact. At this time the internal pressure greatly exceeds that of the surrounding water, and therefore the bubble begins to expand, entering an oscillatory state with

two further cycles of expansion and collapse. Our simulation was halted after the third collapse, however the Gilmore-Akulichev model predicts that when the bubble encounters the tensile portion of the lithotripter pulse it will enter a phase of prolonged expansion, followed by a series of lower-frequency oscillations [2]. This stage of the bubble behaviour will be examined in our future work.

5 Conclusion

The simulation of the near field interaction of a single air bubble with a lithotripter pulse, in axisymmetric form, has been performed using the Free-Lagrange code *Vucalm*. The results showed that the method allows sharp capture of the bubble boundary at all times and successfully predicts many details of the shock/bubble interaction. The impact of the shock on the upstream bubble wall causes it to involute and form a jet of liquid. The jet penetrates the interior of the bubble and strikes the downstream wall, generating a strong near-spherical blast wave into the surrounding fluid. Successive cycles of rebound and collapse occur prior to the long expansion phase, each collapse of the bubble emitting weak pressure waves into the surrounding water. This is predicted by the Gilmore-Akulichev model but has been overlooked by other workers. It is postulated that the liquid jet and strong spherical blast wave may assist in the fragmentation of kidney stones during clinical lithotripsy. Further work has been carried out to examine the influence on initial bubble size, shock strength and the proximity of a solid surface on the behaviour of the bubble. However, due to limited space, this work can not be included in the current paper.

References

1. A.J. Coleman, J.E. Saunders, L.A. Crum, M. Dyson: Ultrasound Med. Biol. **13/2**, 69–76 (1987)
2. C.C. Church: J. Acoust. Soc. Am. **86/1**, 215–227 (1989)
3. A. Phillip, W. Lauterborn: J. Fluid Mech. **361**, 75–116 (1998)
4. N.K. Bourne, J.E. Field: J. Fluid Mech. **244**, 225–240 (1992)
5. L.A. Crum: J. Urol. **140**, 1587–1590 (1988)
6. D. Howard, B. Sturtevant: Ultrasound Med. Biol. **23** 1107–1122 (1997)
7. A.J. Coleman, M.J. Choi, J.E. Saunders, T.G. Leighton: Ultrasound Med. Biol. **18/3**, 267–281 (1992)
8. K.B. Cunningham, A.J. Coleman, T.G. Leighton, P.R. White: Acoustics Bulletin **26/5** 10–16 (2001)
9. P. Zhong, I. Cioanta, F.H. Cocks, G.M. Preminger: J. Acoust. Soc. Am. **101/5**, 2940–2950 (1997)
10. G.J. Ball: Shock Waves **5**, 311–325 (1996)
11. B.P. Howell, G.J. Ball: Shock Waves **10**, 253–264 (2000)
12. G.J. Ball, B.P. Howell, T.G. Leighton, M.J. Schofield: Shock Waves **10**, 265–276 (2000)
13. T.B Benjamin, A.T. Ellis: Phil. Trans. R. Soc. Lond. **A260** 221–240 (1966)